

Oxygen transport and GeO₂ stability during thermal oxidation of Ge

S. R. M. da Silva, G. K. Rolim, G. V. Soares, I. J. R. Baumvol, C. Krug et al.

Citation: *Appl. Phys. Lett.* **100**, 191907 (2012); doi: 10.1063/1.4712619

View online: <http://dx.doi.org/10.1063/1.4712619>

View Table of Contents: <http://apl.aip.org/resource/1/APPLAB/v100/i19>

Published by the [American Institute of Physics](#).

Related Articles

Understanding of the retarded oxidation effects in silicon nanostructures

Appl. Phys. Lett. **100**, 263111 (2012)

Oxidation kinetics of nanoscale copper films studied by terahertz transmission spectroscopy

J. Appl. Phys. **111**, 123517 (2012)

Catalytic behavior of metallic particles in anisotropic etching of Ge(100) surfaces in water mediated by dissolved oxygen

J. Appl. Phys. **111**, 126102 (2012)

Cabrera-Mott kinetics of oxidation of metal nanowires

Appl. Phys. Lett. **100**, 243105 (2012)

Enhanced oxidation of nanoscale In particles at the interface with a Si nanowire

Appl. Phys. Lett. **100**, 231602 (2012)

Additional information on *Appl. Phys. Lett.*

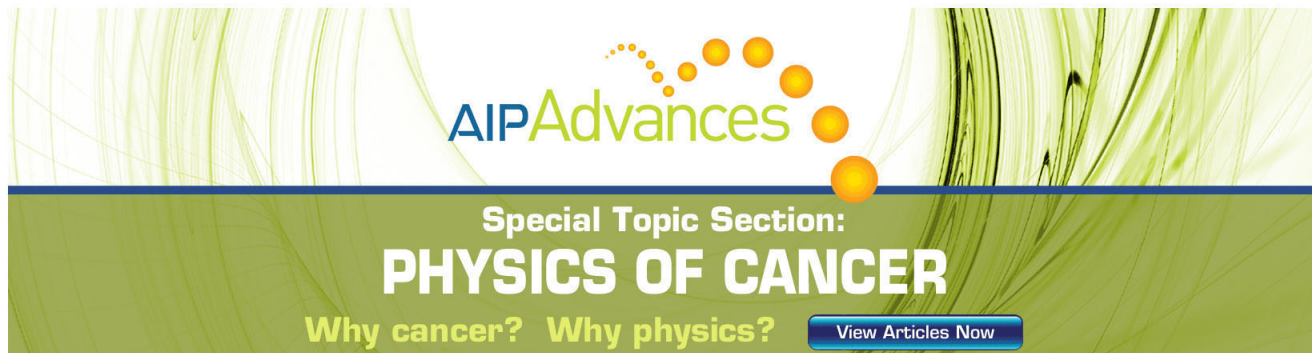
Journal Homepage: <http://apl.aip.org/>

Journal Information: http://apl.aip.org/about/about_the_journal

Top downloads: http://apl.aip.org/features/most_downloaded

Information for Authors: <http://apl.aip.org/authors>

ADVERTISEMENT

The advertisement features a green and white background with abstract, flowing lines. At the top, the 'AIP Advances' logo is displayed, with 'AIP' in blue and 'Advances' in green, accompanied by a series of orange and yellow dots. Below the logo, the text 'Special Topic Section: PHYSICS OF CANCER' is written in white on a dark green background. At the bottom, the phrase 'Why cancer? Why physics?' is written in white, followed by a blue button with the text 'View Articles Now' in white.

Oxygen transport and GeO₂ stability during thermal oxidation of Ge

S. R. M. da Silva,¹ G. K. Rolim,² G. V. Soares,¹ I. J. R. Baumvol,^{1,3} C. Krug,^{1,4} L. Miotti,⁵ F. L. Freire, Jr.,⁶ M. E. H. M. da Costa,⁶ and C. Radtke^{2,a)}

¹Instituto de Física, UFRGS, 91509-900 Porto Alegre, Brazil

²Instituto de Química, UFRGS, 91509-900 Porto Alegre, Brazil

³Universidade de Caxias do Sul, 95070-560 Caxias do Sul, Brazil

⁴CEITEC S.A., 91550-000 Porto Alegre, Brazil

⁵Soprano Ltda, 95180-000 Farroupilha, Brazil

⁶Departamento de Física, PUC-Rio, 22453-900 Rio De Janeiro, Brazil

(Received 23 March 2012; accepted 23 April 2012; published online 9 May 2012)

Oxygen transport during thermal oxidation of Ge and desorption of the formed Ge oxide are investigated. Higher oxidation temperatures and lower oxygen pressures promote GeO desorption. An appreciable fraction of oxidized Ge desorbs during the growth of a GeO₂ layer. The interplay between oxygen desorption and incorporation results in the exchange of O originally present in GeO₂ by O from the gas phase throughout the oxide layer. This process is mediated by O vacancies generated at the GeO₂/Ge interface. The formation of a substoichiometric oxide is shown to have direct relation with the GeO desorption. © 2012 American Institute of Physics.

[<http://dx.doi.org/10.1063/1.4712619>]

Germanium (Ge) is resurging as an interesting material for silicon (Si) replacement in metal-oxide-semiconductor field-effect transistor (MOSFET) technology. It presents the highest hole mobility among all known semiconductor materials, being the leader candidate to replace Si in future PMOS devices.^{1,2} However, finding an efficient passivation route for Ge is still a challenge. Unlike SiO₂ thermally grown on Si, GeO₂ is thermally unstable in processing temperatures usually employed in device fabrication.³ Moreover, it is water soluble and hygroscopic. In view of these characteristics, an apparently trivial solution is the replacement of the Ge native oxide by another dielectric material with intrinsically superior physical properties. A higher dielectric constant material is the natural choice aiming at device scaling. Nevertheless, the direct deposition of high-k materials on Ge gave rise to undesirable effects. Atomic layer deposition (ALD) of HfO₂ on a Ge surface after wet chemical treatment resulted in quasiepitaxial growth.⁴ Ge incorporation to the dielectric layer was observed with time-of-flight secondary ion mass spectrometry (TOF-SIMS)⁵ and was related to an increase in interface trap density. These and other results evidence deleterious effects of the direct deposition of HfO₂ on Ge pointing to the need of interlayers (ILs) between these materials.⁶

Different materials were already investigated as potential ILs for dielectric stacks deposited on Ge. La₂O₃ in conjunction with ZrO₂ caps formed a stable structure on Ge with good electrical properties.⁷ Relatively low interface state density values ($D_{it} \sim 3 \times 10^{11} \text{ cm}^{-2} \text{ eV}^{-1}$) were obtained using Al₂O₃ ILs.⁸ Thermally grown GeO₂ was also proposed to be a good IL for high-k dielectrics deposited by means of ALD.⁹ Independently of the passivation strategy, Ge substrate oxidation can occur during deposition of the dielectric material and/or device processing.^{10–12} Thus, understanding (i) the mechanisms involved in the thermal oxidation of Ge and (ii) the related GeO desorption is crucial in order to control the properties of gate dielectric stacks.

Wang and coworkers^{13,14} investigated GeO desorption in detail. They concluded that this process is not a result of the decomposition of GeO₂ itself below 700 °C but of the reaction of GeO₂ with the Ge substrate. The absence of GeO desorption from GeO₂/SiO₂/Si structures corroborated this conclusion. The consumption of Ge underneath GeO₂ occurs via the GeO₂ + Ge → GeO reaction, as evidenced by the decomposition of line-patterned GeO₂/Ge stacks. Moreover, based on isotopic tracing results, it was demonstrated that Ge and O in the desorbed GeO come from the GeO₂ surface. Estimating the diffusion coefficients of Ge and O in isotopically labeled GeO₂/Ge structures, it was shown that O presents a much higher diffusivity. Thus, O motion was considered dominant in GeO₂. Based on all these observations, an oxygen vacancy diffusion model was proposed. According to this model, oxygen vacancies are generated from the interfacial redox reaction between GeO₂ and Ge. Since the equilibrium concentration of oxygen vacancies is much higher for the interfacial region than for the GeO₂ bulk, oxygen vacancies diffuse towards the GeO₂ surface promoting further GeO desorption.

All of these conclusions were drawn from experiments performed in vacuum conditions without the presence of oxidizing agents that could modify the GeO desorption. The use of different oxidizing atmospheres was shown to have beneficial effects on the electrical properties of dielectric/Ge structures amending electrically active defects. Such treatments include the use of wet N₂,¹⁵ high pressure water treatment using supercritical fluids,¹⁶ post metal annealing in an oxygen/nitrogen mixture,¹⁷ and high pressure (70 atm) O₂.¹⁸ The observed improvements may be due to the suppression of GeO desorption and to modifications of the original dielectric layer. In view of this scenario, we investigated GeO desorption and other mechanisms involved in the thermal oxidation of Ge in dry oxygen. The main objectives were to identify the influence of oxidation parameters (oxygen pressure and temperature) on the amount of desorbed Ge and to understand oxygen transport mechanisms taking place during Ge thermal oxidation.

^{a)}Electronic mail: claudio@iq.ufrgs.br.

Starting samples were p-type epitaxial Ge (100) wafers doped with Ga (Umicore), with a resistivity of 0.24–0.47 Ω cm. They were first cleaned in an ultrasonic acetone bath, and then followed a cleaning procedure with H_2O_2 and HCl aqueous solutions.¹⁹ ^{18}O (100) samples were cleaned in a mixture of H_2SO_4 and H_2O_2 followed by etching in a 40% HF aqueous solution for 1 min. After rinsing the samples in deionized water, they were immediately transferred to load lock chambers. Ge thermal oxidations were performed in a resistively heated quartz tube furnace that was pumped down to 2×10^{-7} mbar and then pressurized with O_2 enriched or not to 97% in the ^{18}O rare isotope (termed $^{18}\text{O}_2$). Stoichiometric GeO_2 layers were deposited on Si substrates in a remote plasma enhanced chemical vapor deposition (RPECVD) reactor. In order to probe the influence of germanium oxide stoichiometry on its thermal stability, we deposited substoichiometric GeO layers on Si by pulsed DC reactive magnetron sputtering using a Ge target. Deposition parameters were optimized to produce a GeO layer as checked by Rutherford backscattering spectrometry (RBS). Ge desorption during GeO_2 thermal growth was tracked by placing a thermally oxidized Si sample on top of the Ge substrate.²⁰ Depth distributions of ^{18}O were obtained by nuclear reaction profiling (NRP) using the resonance at 151 keV in the cross section curve of the $^{18}\text{O}(p,\alpha)^{15}\text{N}$ nuclear reaction.²¹ ^{18}O and ^{16}O areal densities were determined by nuclear reaction analysis (NRA) using the plateau regions in the cross section curves of the $^{18}\text{O}(p,\alpha)^{15}\text{N}$ (730 keV incident protons) and $^{16}\text{O}(D,p)^{17}\text{O}$ (810 keV incident deuterons) nuclear reactions, respectively. Ge amounts adsorbed on the Si samples were determined by RBS using He^+ ions of 1 MeV.

^{18}O areal densities of Ge samples as a function of the oxidation temperature are shown in the upper part of Fig. 1. Oxidations were performed under three different $^{18}\text{O}_2$ pressures. Higher oxidation temperatures resulted in thicker oxide films for samples oxidized under 1 atm. This result is consistent with the acceleration of GeO_2 formation. The right vertical axis corresponds to the equivalent oxide thickness assuming a GeO_2 density of 3.6 g/cm^3 .²² A contrasting behavior is observed for 100 and 200 mbar. At 600°C , ^{18}O is not detected within the sensitivity of NRA for these oxygen pressures. This result evidences that besides oxide formation, there is another mechanism taking place in parallel. From previous studies,¹³ it is known that GeO desorption occurs in this temperature range. In order to confirm and quantify this desorption, we placed a thermally oxidized Si substrate above the Ge sample in order to adsorb Ge containing species eventually desorbed from the underlying Ge sample.²⁰ The amount of adsorbed Ge determined by RBS for each oxidation condition is shown in the lower part of Fig. 1. Higher temperatures and lower oxygen pressures promote GeO desorption. If one calculates the ratio between the amount of Ge adsorbed on SiO_2 (Fig. 1(b)) and the amount of Ge in the GeO_2 film obtained from Fig. 1(a), an estimation of the fraction of oxidized Ge that is desorbed can be obtained. For the Ge sample oxidized at 600°C under 1 atm, this fraction is 0.19, indicating that a substantial part of Ge that is oxidized actually desorbs. It is worth to mention that this value is underestimated since Ge species desorbed from the Ge substrate not necessarily adsorb on the Si sample. At

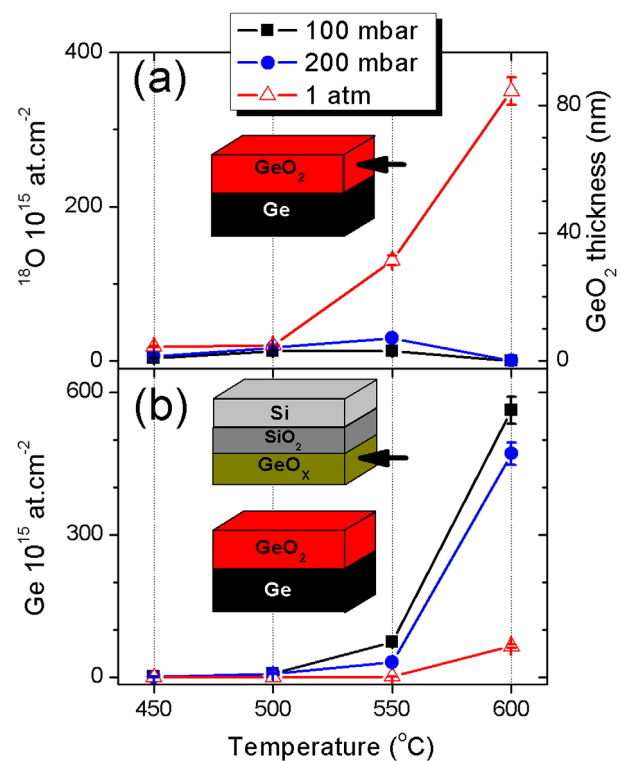


FIG. 1. (a) ^{18}O areal densities as a function of the oxidation temperature. Ge substrates were oxidized for 2 h under different $^{18}\text{O}_2$ pressures as indicated. The right vertical axis corresponds to the respective oxide thickness obtained assuming a GeO_2 density of 3.6 g/cm^3 . (b) Ge areal densities obtained from Si samples placed above the Ge substrates during thermal oxidation. A sketch of the sample positioning is shown in each part of the figure indicating the analyzed sample. Lines are only to guide the eyes. 5% error bars are included.

600°C , oxidation in low oxygen pressures (100 and 200 mbar) resulted in the complete volatilization of oxidized Ge, corresponding to the active oxidation regime of the Ge substrate.¹³ All these observations evidence the influence of oxygen pressure and temperature in the Ge thermal oxidation process.

Oxygen incorporation and desorption during Ge thermal oxidation were investigated using isotopic tracing. GeO_2 films were thermally grown on Ge using $^{16}\text{O}_2$. These samples underwent a second oxidation step in $^{18}\text{O}_2$ for different times. The amounts of ^{16}O and ^{18}O were determined for each sample by NRA and are shown in Fig. 2. Squares in the graph indicate the total oxygen areal concentration ($^{16}\text{O} + ^{18}\text{O}$). This value increases for longer reoxidation times in $^{18}\text{O}_2$, indicating that oxide growth takes place under these oxidation conditions. ^{16}O originally present in the starting sample is lost: the longer the reoxidation, the higher the ^{16}O loss. In contrast, increasing ^{18}O areal densities are observed. These observations show that O originally present in the GeO_2 layer is replaced by oxygen from the gas phase during Ge thermal oxidation.

In order to understand the mechanisms underlying oxygen isotopic exchange, we performed ^{18}O depth profiling. Fig. 3 shows nuclear reaction data regarding ^{18}O in GeO_2/Ge samples. A reference sample was prepared growing a GeO_2 thermal oxide on Ge using $^{18}\text{O}_2$. The others are those of Fig. 2: Ge substrates oxidized in $^{16}\text{O}_2$ followed by a reoxidation in $^{18}\text{O}_2$. Alpha particle yield in the figure is proportional to ^{18}O concentration; depth in the sample scales with proton

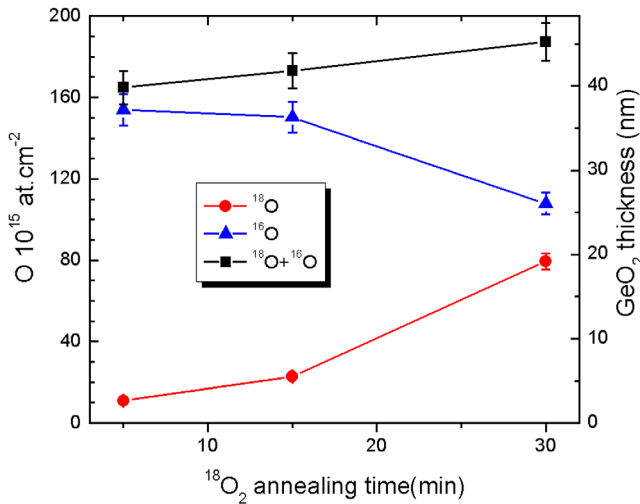


FIG. 2. O areal densities as a function of the reoxidation time in $^{18}\text{O}_2$. Samples were prepared by a first oxidation step in 1 atm of $^{16}\text{O}_2$ for 15 min at 600°C . Reoxidations were performed in 1 atm of $^{18}\text{O}_2$ at 600°C . The right vertical axis corresponds to the respective oxide thickness obtained assuming a GeO_2 density of 3.6 g/cm^3 .

energy. The curves shown correspond to the actual concentration versus depth information convoluted with instrumental and proton energy loss functions. GeO_2 surface and GeO_2/Ge interface positions can be estimated by the energy position of the leading and trailing edges of the excitation curves, respectively. The maximum alpha yield obtained with the $\text{Ge}^{18}\text{O}_2/\text{Ge}$ sample corresponds to the ^{18}O concentration in stoichiometric GeO_2 . Results obtained for the sample reoxidized for 5 min evidence ^{18}O incorporation throughout the previously formed GeO_2 layer. For longer times, higher ^{18}O concentrations are observed. This observation is in agreement with the diffusion of oxygen vacancies towards the GeO_2 surface which constitute incorporation sites for incoming ^{18}O from the gas phase. Additional results

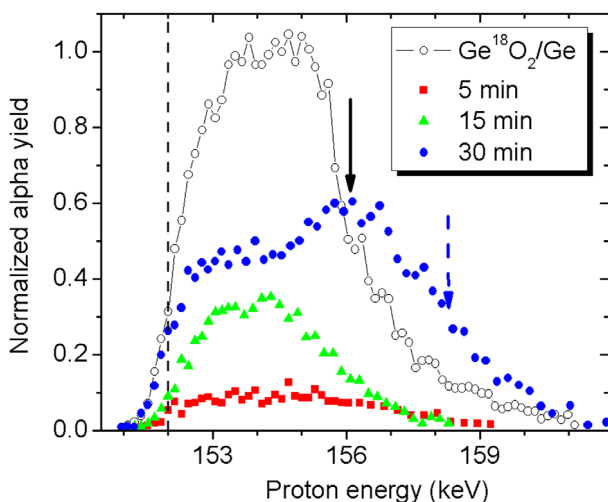


FIG. 3. Experimental excitation curves of the $^{18}\text{O}(p,\alpha)^{15}\text{N}$ nuclear reaction for (i) a reference sample prepared by thermally oxidizing Ge in 1 atm of $^{18}\text{O}_2$ for 15 min at 600°C and (ii) samples prepared with the same conditions but using $^{16}\text{O}_2$ followed by a reoxidation step in $^{18}\text{O}_2$ for the times indicated in the figure. An estimation of the proton energy corresponding to the GeO_2 surface is indicated by a dashed line. The energy position of GeO_2/Ge interfaces of the reference sample and of that reoxidized for 30 min are indicated by a solid and a dashed arrow, respectively.

presented in the following confirm that oxygen vacancies generated in the GeO_2/Ge interface are responsible for this ^{18}O incorporation. The longer the reoxidation time, the higher the oxygen isotopic exchange in the GeO_2 layer, in agreement with NRA results of Fig. 2. An additional feature is observed for the sample reoxidized for 30 min: ^{18}O accumulation takes place close to the GeO_2/Ge interface. This observation is related to the formation of new GeO_2 which results in a thicker oxide layer, as evidenced by the deeper GeO_2/Ge interface position, as well as a increase in the total oxygen amount ($^{16}\text{O} + ^{18}\text{O}$) presented in Fig. 2.

To elucidate the role played by O vacancies in ^{18}O incorporation, we performed an investigation of the interaction of oxygen from the gas phase with GeO_2 , without or at least with a reduced concentration of such vacancies. For that purpose, we deposited a stoichiometric 10 nm thick GeO_2 layer on SiO_2/Si by RPECVD. In this way, there is no interfacial redox reaction between GeO_2 and Ge, which is the source of O vacancies in such structures. These samples were annealed in 1 atm of $^{18}\text{O}_2$ at 600°C for 1 h. Fig. 4 shows the experimental excitation curve of the $^{18}\text{O}(p,\alpha)^{15}\text{N}$ nuclear reaction and the corresponding simulation for this sample. With such a thinner oxide sample, we were able to simulate the excitation curve (with a model that takes into account the ion energy loss as well as other relevant experimental contributions²¹) and obtain the ^{18}O profile (also shown in Fig. 4). ^{18}O depth distribution shows that, as in the case of GeO_2/Ge samples, there is also ^{18}O incorporation throughout the GeO_2 layer. However, this isotope is incorporated in a much lesser extent: around 13% of the O concentration in stoichiometric GeO_2 against 50% in the case of GeO_2/Ge . It is worth to mention that the $\text{GeO}_2/\text{SiO}_2/\text{Si}$ sample was oxidized in $^{18}\text{O}_2$ for a longer time: twice the longest reoxidation time of GeO_2/Ge samples.

The present results evidence that O vacancies play a decisive role in the oxygen transport from the gas phase towards the GeO_2/Ge interface, incorporating O in the GeO_2 bulk region. The creation of such vacancies is also related to

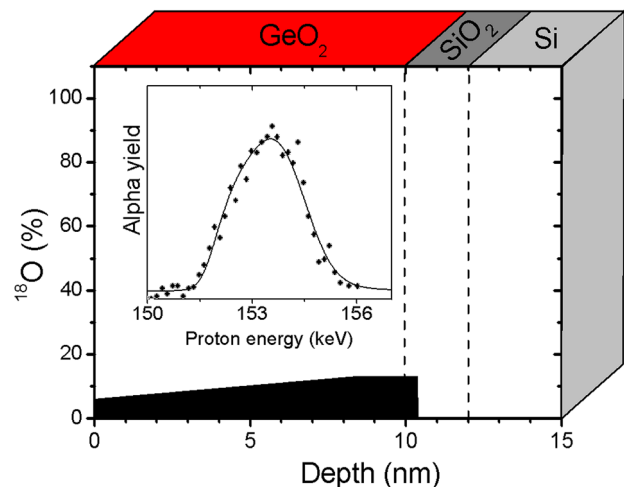


FIG. 4. ^{18}O profile assumed in the simulation of nuclear reaction data. In the inset is shown the experimental excitation curve (symbols) and the corresponding simulation (line) for a $\text{GeO}_2/\text{SiO}_2/\text{Si}$ sample prepared by RPECVD annealed in 1 atm of $^{18}\text{O}_2$ for 1 h at 600°C . A sketch of the sample structure is shown.

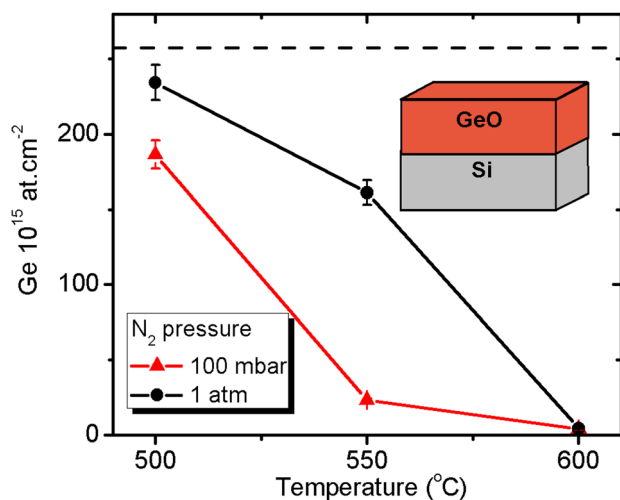


FIG. 5. Reminiscent Ge areal densities of GeO/Si samples prepared by DC reactive magnetron sputtering submitted to N₂ annealing. Samples were annealed for 2 h under N₂ pressures indicated in the figure at three different temperatures. The horizontal dashed line corresponds to the Ge areal density of the samples prior to the annealing step. Areal densities were determined by RBS. A sketch of the sample used in the experiment is shown. Lines are only to guide the eyes. 5% error bars are included.

the formation of nonstoichiometric Ge oxides at the dielectric surface which are believed to promote volatilization of Ge species. In order to confirm that volatilization is related to the Ge oxide stoichiometry, we performed a desorption experiment. GeO layers were deposited on Si and annealed in N₂ atmosphere. Fig. 5 shows the remaining Ge areal concentrations following annealing as a function of temperature with pressure as a parameter. A clear reduction of the Ge areal concentration is observed. N₂ pressure and temperature have the same influence as in the case of thermal oxidation. The absence of desorption up to 550 °C was observed with stoichiometric GeO₂ layers deposited on SiO₂.²³ These contrasting results evidence the role of the Ge oxide stoichiometry in its thermal stability.

In summary, we investigated oxygen transport during thermal oxidation of Ge and desorption of the formed Ge oxide. Higher oxidation temperatures and lower oxygen pressures promote GeO desorption. A considerable fraction of oxidized Ge desorbs during the growth of the GeO₂ layer, this fraction being a function of oxidizing parameters. This fraction varies gradually with the oxidation parameters in contrast to the sharp transition between oxide growth and semiconductor substrate etching observed for Si thermal oxidation.²⁴ The interplay between oxygen desorption and incorporation results in the exchange of O originally present in GeO₂ by O from the gas phase, throughout the oxide layer. This process is mediated by O vacancies generated at the GeO₂/Ge interface which diffuse towards the GeO₂ surface. This mechanism also promotes the formation of a substoichiometric oxide which is the source of GeO desorption. This process can be controlled by varying the O supply at the GeO₂ surface via O₂ pressure. These observations evidence fundamental differences between the thermal oxida-

tion of Si and Ge. In the former case, oxide growth occurs via the interstitial transport of O from the gas through the growing oxide without reaction with the oxide matrix. O exchange was shown to occur only at the SiO₂ surface and at the SiO₂/Si interface²⁵ in striking contrast to GeO₂ thermal growth. The present results evidence the central role played by the GeO₂ stability in future PMOS devices based on Ge. Oxygen uptake at the GeO₂ surface can be tuned by varying the conditions of processing steps aiming at healing possible sources of instabilities. Besides this fact, a careful choice of the material deposited on GeO₂ must be done: reduction of GeO₂ by deposited layers (Hf, for example, Ref. 23) can also promote desorption of Ge species.

This work was funded by INCT Namitec, INCT INES, MCT/CNPq, CAPES, and FAPERGS.

- ¹R. Pillarisetty, *Nature* **479**, 324 (2011)
- ²A. Lubow, S. Ismail-Beigi, and T. P. Ma, *Appl. Phys. Lett.* **96**, 122105 (2010).
- ³Y. Kamata, *Mater. Today* **11**, 30 (2008).
- ⁴E. P. Gusev, H. Shang, M. Copel, M. Gribelyuk, C. D'Emic, P. Kozlowski, and T. Zabel, *Appl. Phys. Lett.* **85**, 2334 (2004).
- ⁵Q. Zhang, N. Wu, D. M. Y. Lai, Y. Nikolai, L. K. Bera, and C. Zhu, *J. Electrochem. Soc.* **153**, G207 (2006).
- ⁶A. Delabie, F. Bellenger, M. Houssa, T. Conard, S. V. Elshocht, M. Caymax, M. Heyns, and M. Meuris, *Appl. Phys. Lett.* **91**, 82904 (2007).
- ⁷G. Mavrou, P. Tsipas, A. Sotiropoulos, S. Galata, Y. Panayiotatos, A. Dimoulas, C. Marchiori, and J. Fompeyrine, *Appl. Phys. Lett.* **93**, 212904 (2008).
- ⁸S. Swaminathan, M. Shandalov, Y. Oshima, and P. C. McIntyre, *Appl. Phys. Lett.* **96**, 82904 (2010).
- ⁹A. Delabie, F. Bellenger, M. Houssa, T. Conard, S. V. Elshocht, M. Caymax, M. Heyns, and M. Meuris, *Appl. Phys. Lett.* **91**, 82904 (2007).
- ¹⁰C. Radtke, N. M. Bom, G. V. Soares, C. Krug, and I. J. R. Baumvol, *ECS Trans.* **41**(3), 21 (2011).
- ¹¹C. Radtke, C. Krug, G. V. Soares, I. J. R. Baumvol, J. M. J. Lopes, E. Durgun-Ozben, A. Nichau, J. Schubert, and S. Mantl, *Electrochem. Solid-State Lett.* **13**, G37 (2010).
- ¹²C. Henkel, O. Bethge, S. Abermann, S. Puchner, H. Hutter, and E. Bertagnolli, *Appl. Phys. Lett.* **91**, 82904 (2007).
- ¹³S. K. Wang, K. Kita, C. H. Lee, T. Tabata, T. Nishimura, K. Nagashio, and A. Toriumi, *J. Appl. Phys.* **108**, 054104 (2010).
- ¹⁴S. K. Wang, K. Kita, T. Nishimura, K. Nagashio, and A. Toriumi, *Jpn. J. Appl. Phys.* **50**, 04DA01 (2011).
- ¹⁵X. Zou, J. P. Xu, C. X. Li, and P. T. Lai, *Appl. Phys. Lett.* **90**, 163502 (2007).
- ¹⁶C.-S. Huang and P.-T. Liul, *Appl. Phys. Lett.* **99**, 82907 (2011).
- ¹⁷S. Deng, Q. Xie, D. Deduytsche, M. Schaeckers, D. Lin, M. Caymax, A. Delabie, S. V. den Berghe, X. Qu, and C. Detavernier, *Appl. Phys. Lett.* **99**, 52906 (2011).
- ¹⁸C. H. Lee, T. Tabata, T. Nishimura, K. Nagashio, K. Kita, and A. Toriumi, *Appl. Phys. Express* **2**, 71404 (2009).
- ¹⁹H. Okumura, T. Akane, and S. Matsumoto, *Appl. Surf. Sci.* **125**, 125 (1998).
- ²⁰Y. Oniki, H. Koumo, Y. Iwazaki, and T. Ueno, *J. Appl. Phys.* **107**, 124113 (2010).
- ²¹C. Driemeier, L. Miotti, R. P. Pezzi, K. P. Bastos, and I. J. R. Baumvol, *Nucl. Instrum. Methods Phys. Res. B* **249**, 278 (2006).
- ²²Y. Y. Huang, A. Sarkar, and P. C. Schultz, *J. Non-Cryst. Solids* **27**, 29 (1978).
- ²³H. Koumo, Y. Oniki, Y. Iwazaki, and T. Ueno, *J. Electrochem. Soc.* **158**, G146 (2011).
- ²⁴F. W. Smith and G. Ghidini, *J. Electrochem. Soc.* **129**, 1301 (1982).
- ²⁵T. Akermark, L. G. Gosset, J. J. Ganem, I. Trimaille, I. Vickridge, and S. Rigo, *J. Appl. Phys.* **86**, 1153 (1999).